Advances in Aircraft and Spacecraft Science, *Vol. 13, No. 2 (2026) 195-215*
https://doi.org/10.12989/aas.2026.13.2.195

Techno-Press

A refined shear deformation model for mechanical buckling analysis of functionally graded transparent architectural shell structures

Djilalli Mokhefi[1], Ahmed Bakoura[2,3], Fouad Kherbouche[4], Ali Belhocine[1], Ahmed Amine Daikh[1,5], Mohammed Sid Ahmed Houari*[1]

[1]*Laboratoire d'Etude des Structures et de Mécanique des Matériaux, Département de Génie Civil, Faculté des Sciences et de la Technologie, Université Mustapha Stambouli B.P. 305, R.P. 29000 Mascara, Algérie*
[2]*Département de Génie Civil, Faculté d'Architecture et de Génie Civil, Université des Sciences et de la Technologie d'Oran, BP 1505 El M'naouer, USTO, Oran, Algeria*
[3]*Material and Hydrology Laboratory, Civil Engineering Department, Faculty of Technology, University of Sidi Bel Abbes, Algeria*
[4]*Laboratory of Science and Technology of Water (LSTE), Department of Electrical Engineering, University of Mustapha Stambouli, Mascara, BP 305, Algeria*
[5]*Artificial Intelligence Laboratory for Mechanical and Civil Structures, and Soil, University Centre of Naama, Naama, Algeria*

(Received March 15, 2026, Revised June 16, 2026, Accepted June 20, 2026)

Abstract. This study introduces a refined and computationally efficient hyperbolic Shear-Order Shear Deformation Theory (HypSDT) with only four displacement variables for the buckling analysis of functionally graded transparent (FGT) doubly curved shells. By reducing the number of unknowns compared with conventional FSDT formulations, the proposed model achieves high accuracy while improving computational efficiency. The analysis focuses on shells made of sapphire and soda lime glass, and the governing equations are derived using Minimum Total Potential Energy's principle before being solved analytically through the Navier approach for simply supported boundary conditions. The numerical results show that the critical buckling load is highly sensitive to the material gradation index, with higher values of k leading to lower stiffness and reduced buckling resistance. The study also reveals that spherical shells provide the greatest structural stability because of their balanced double curvature, whereas biaxial loading and larger radius-to-side ratios significantly decrease the buckling capacity. Overall, the proposed formulation provides an accurate and efficient tool for the design and analysis of lightweight, transparent shell structures intended for modern architectural and advanced aerospace applications.

Keywords: analytical solution; doubly curved shells; functionally graded materials; refined hyperbolic shear deformation theory; sapphire; soda-lime glass ; structural stability; transparent shells

1. Introduction

The growing demand for transparent structural systems has made curtain walls an essential lement of modern architecture. Their aesthetic appeal, ability to maximize natural daylight, and

*Corresponding author, Professor, E-mail: ms.houari@univ-mascara.dz

Copyright © 2026 Techno-Press
http://www.techno-press.org/aas/5
ISSN: 2287-528X (Print), 2287-5271 (Online)

contribution to occupant comfort has led to their widespread adoption in contemporary buildings. Typically composed of double- or triple-glazed panels, these systems are designed to ensure structural integrity while providing excellent thermal and environmental performance. Despite their widespread application, conventional multilayer glazing systems exhibit several inherent limitations, such as increased self-weight, complex manufacturing processes, and durability concerns arising from the interfaces between adjacent layers. These challenges have motivated growing research efforts toward the development of innovative transparent structural systems offering enhanced mechanical performance while maintaining the functional and architectural benefits of traditional glazing [1], [2].

In this context, functionally graded materials (FGMs) have received significant attention over the past decades due to their unique ability to provide a continuous variation of material properties across the thickness of structural components. Unlike conventional laminated composites, FGMs avoid sharp interfaces between different constituents, thereby reducing interlaminar stresses and enhancing overall structural reliability [3], [4]. Owing to these advantages, FGMs have been widely adopted in various engineering fields, including aerospace structures, thermal barrier coatings, and advanced composite systems. More recently, the development of functionally graded transparent materials has emerged as a promising strategy for designing innovative transparent structural components that combine high optical transparency with improved mechanical performance and durability [5-7].

In parallel, lightweight composite structures have attracted increasing interest due to their superior strength-to-weight ratio, enhanced durability, and wide range of applications in aerospace, civil, marine, and mechanical engineering. Among these structures, functionally graded plates and shells offer additional benefits by enabling a smooth transition of material properties, which contributes to improved load-carrying capacity and reduced stress concentrations. As emphasized in the recent review by Liu et al. [8], accurately predicting the static, buckling, and vibration responses of advanced composite structures remains a challenging issue due to the combined effects of complex geometries, material heterogeneity, and nonlinear structural behavior. Therefore, the development of refined, accurate, and computationally efficient theoretical models remains an active research direction for the analysis and optimal design of next-generation shell structures.

From the perspective of structural mechanics, the stability and vibration responses of functionally graded (FG) plates and shells have been extensively studied over the past decades. Numerous theoretical approaches have been developed, including the Classical Plate Theory (CPT), First-Order Shear Deformation Theory (FSDT), and various Higher-Order Shear Deformation Theories (HSDTs). However, many existing formulations require five or more displacement variables, which may lead to increased computational complexity, particularly when dealing with shells involving complex geometries and multiphysical effects.

The Classical Plate Theory neglects transverse shear deformation effects and is therefore mainly applicable to thin structural elements such as Alashkar et al. [9]. Several investigations have employed CPT to examine the mechanical behavior of FG plates and shells. Arefi [10] studied the free vibration characteristics of FG circular plates integrated with piezoelectric layers, while Darılmaz [11] analyzed FG grid structures using a hybrid-stress finite element formulation. Pradhan et al. [12] investigated the vibration behavior of FG elliptic plates under different boundary conditions, and Moita et al. [13] examined the mechanical and thermal buckling responses of FG axisymmetric plate-shell structures. In addition, extensive studies have addressed the buckling and vibration behavior of advanced composite and orthotropic plates, highlighting the

influence of porosity, material distribution, loading conditions, and elastic foundations on structural performance [14-18].

To overcome the limitations of CPT, the First-Order Shear Deformation Theory (FSDT) was introduced by incorporating transverse shear deformation effects. This theory assumes a linear distribution of displacements through the thickness and provides reliable predictions for both thin and moderately thick shells. However, because FSDT assumes constant transverse shear strains, a shear correction factor is required. The accurate determination of this factor remains challenging since it depends on several parameters, including geometry, material properties, and boundary conditions [19], [20]. Despite this limitation, FSDT has been widely adopted for analyzing FG shell structures. Madani et al. [21] investigated FG carbon nanotube-reinforced piezoelectric cylindrical shells under thermal loading using FSDT combined with the differential cubature method. Qin et al. [22] proposed a unified formulation for the free vibration analysis of graphene platelet-reinforced FG shallow shells with arbitrary boundary conditions. Li et al. [23], [24] developed semi-analytical FSDT-based models to study the vibration characteristics of FG porous cylindrical, spherical, and laminated shells under complex boundary conditions.

To achieve higher accuracy while avoiding the limitations associated with the shear correction factor, Higher-Order Shear Deformation Theories (HSDTs) have been developed. These theories satisfy the zero transverse shear stress conditions at the top and bottom surfaces of the structure, eliminating the need for correction factors. Kar et al. [25] investigated the buckling behavior of FG curved shell panels using HSDT combined with finite element analysis, while Kar et al. [26] studied the thermal post-buckling response of FG shallow curved shells. Kar and Panda [27] analyzed the nonlinear vibration behavior of FG spherical panels using HSDT with nonlinear kinematic relations.

Recent developments have further extended FG shell theories toward multiphysics and nonlinear analyses. Liu et al. [28] investigated nonlinear forced vibrations and bifurcation phenomena of FG piezoelectric cylindrical shells subjected to coupled electric-thermo-mechanical loading, demonstrating the significant role of material gradation and coupled-field effects on structural behavior. These studies emphasize the importance of refined shell theories capable of accurately predicting the stability and dynamic responses of advanced FG structures under complex loading conditions.

More recently, HSDT formulations have been applied to porous orthotropic laminated doubly curved shells to investigate their vibration and stability characteristics [29-33]. Additional contributions by [34-37] have further advanced the understanding of buckling, vibration, and stability behaviors of FG plates and shells under various mechanical and environmental conditions.

In parallel with these developments, several refined higher-order theories have been proposed to reduce computational requirements while maintaining high predictive accuracy. Carrera and Brischetto [38] developed closed-form solutions within Carrera's Unified Formulation to investigate thickness-locking effects in different shell theories, including classical, first-order, higher-order, mixed, and layer-wise approaches. Their results demonstrated that thickness locking occurs only when the transverse normal strain is assumed constant through the thickness and is independent of shell curvature. Thai and Choi [39] introduced various HSDTs based on cubic, sinusoidal, hyperbolic, and exponential functions by decomposing the transverse displacement into bending and shear components. Jung et al. [40] proposed a four-variable refined HSDT for the vibration analysis of S-FGM plates resting on elastic foundations, while Fahsi et al. [41] developed

an efficient nth-order theory using undetermined integral terms with only four displacement variables. These approaches provided an effective compromise between computational efficiency and solution accuracy. More recently, Arefi et al. [42] proposed a higher-order sinusoidal shear theory for bending analysis of composite doubly curved nanoshells with thickness stretching. Civalek and Jalaei [43] investigated the shear buckling response of FG and carbon nanotube-reinforced composite plates, whereas Arshid et al. [44] studied the thermal-elastic buckling and vibration characteristics of three-layer FG structures reinforced with graphene platelet-enhanced composite surfaces.

Despite the extensive research devoted to FG plates and shells, investigations on functionally graded transparent shell structures remain very limited. Moreover, most existing FSDT and HSDT formulations involve a relatively large number of unknown variables, resulting in increased computational effort. Therefore, developing simplified yet accurate theoretical models with fewer degrees of freedom remains an important research challenge. Compared with conventional five-variable FSDT models and advanced higher-order approaches such as HSDT and Carrera's Unified Formulation [45], the present four-variable FSDT model reduces the number of governing unknowns while retaining the ability to account for transverse shear deformation effects. This leads to simpler governing equations, reduced computational cost, and easier numerical implementation while maintaining satisfactory accuracy for the buckling analysis of moderately thick shell structures.

Motivated by these considerations, the present study proposes a refined four-variable hyperbolic HSDT formulation for the mechanical buckling analysis of functionally graded transparent doubly curved shells. The proposed model considers the continuous variation of material properties through the thickness and is applicable to different shell geometries. By reducing the number of displacement variables compared with conventional theories, the proposed approach achieves improved computational efficiency without sacrificing the essential mechanical characteristics required for accurate stability predictions. The governing equations are derived using a variational approach, and the effects of material gradation and geometric parameters on the critical buckling response are systematically investigated.

2. Theoretical formulation

2.1 Functionally graded transparent doubly curved shells

Consider a doubly curved shallow shell made of functionally graded transparent materials (FGTMs), composed of a mixture of ceramic and metal phases. The principal radius of curvature along the x-axis is denoted by R_1, while the principal radius along the y-axis is represented by R_2. The geometric configuration of the shell is illustrated in Fig. 1.

y varying the curvature parameters of the shell, several special types of shell structures can be obtained as follows:

For $R_1 = R_2 \rightarrow \infty$: the shell reduces to a flat plate (FL plate).

For $R_1 = R_2$: the shell becomes a spherical shell (SP shell).

For $R_1 = -R_2$: the shell becomes a hyperbolic paraboloid shell (HP shell).

For $R_2 \rightarrow \infty$: the shell reduces to a cylindrical shell (CY shell).

These four shell configurations are illustrated in Fig. 2.

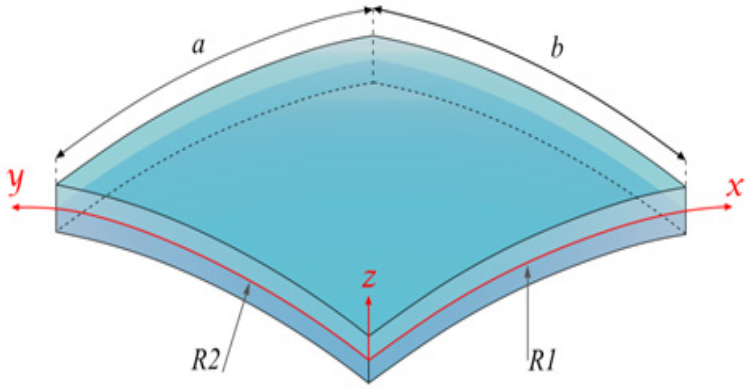

Figure 1. The geometry of the FG transparent doubly curved

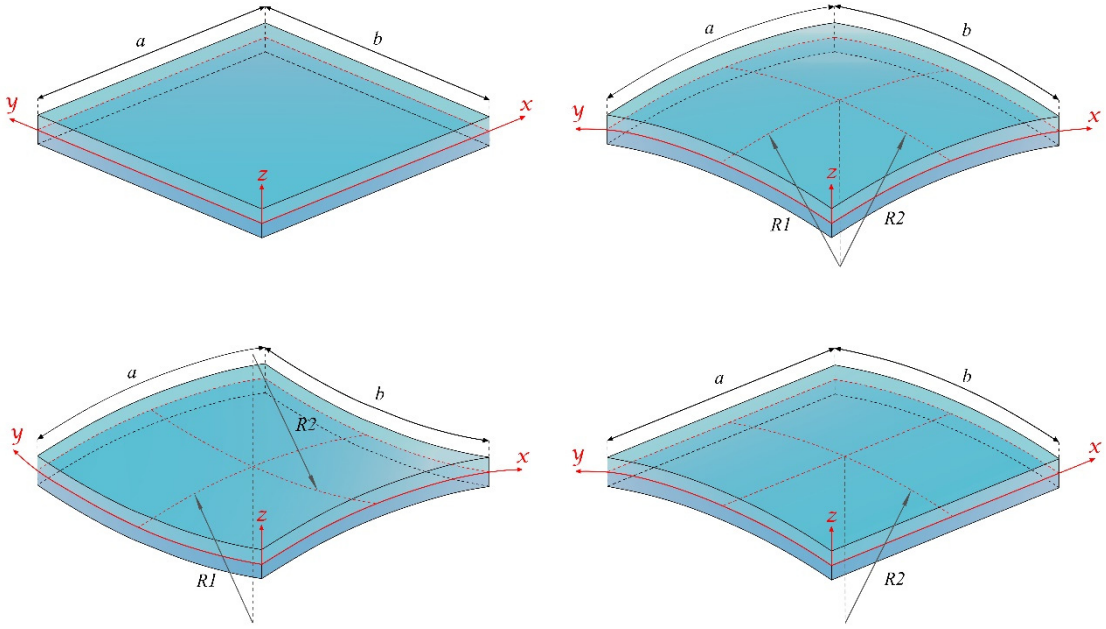

Figure 2. Four types of FG transparent doubly curved shells

2.2 Refined Hyperbolic shear deformation theory

2.2.1 Functionally graded material

Functionally graded materials (FGMs) exhibit a continuous variation of material properties through the thickness of the shell, with the microstructure gradually transitioning from the ceramic phase to the metal phase. Consequently, the effective material properties of the FG shells, such as Young's modulus E, mass density ρ, and Poisson's ratio v, vary smoothly through the thickness according to the volume fraction distribution of the ceramic and metal constituents. Based on the rule of mixtures [46], the effective material properties of the FG shells can be expressed as follows, where the subscripts and denote the ceramic and metal phases, respectively

$$E(z) = E_m + (E_c - E_m)\left(\frac{z}{h} + \frac{1}{2}\right)^k \tag{1a}$$

$$\rho(z) = \rho_m + (\rho_c - \rho_m)\left(\frac{z}{h} + \frac{1}{2}\right)^k \tag{1b}$$

$$v(z) = v_m + (v_c - v_m)\left(\frac{z}{h} + \frac{1}{2}\right)^k \tag{1c}$$

2.2.2 A refined shear deformation theory

In the present study, the displacement field of the shell is described based on a refined first-order shear deformation theory as follows

$$u(x,y,z) = u_0(x,y) - z\frac{\partial w_b}{\partial x} - \Psi(z)\frac{\partial w_s}{\partial x} \tag{2a}$$

$$v(x,y,z) = v_0(x,y) - z\frac{\partial w_b}{\partial y} - \Psi(z)\frac{\partial w_s}{\partial y} \tag{2b}$$

$$w(x,y,z) = w_b(x,y) + w_s(x,y) \tag{2c}$$

In the case of shallow shells, the strain components should include the effects of shell curvatures. Accordingly, the strain field of the shell can be expressed as follows

$$\varepsilon_x = \frac{\partial u_0}{\partial x} - z\frac{\partial^2 w_b}{\partial x^2} - \Psi(z)\frac{\partial^2 w_s}{\partial x^2} + \frac{w_b + w_s}{R_1} \tag{3a}$$

$$\varepsilon_y = \frac{\partial v_0}{\partial y} - z\frac{\partial^2 w_b}{\partial y^2} - \Psi(z)\frac{\partial^2 w_s}{\partial y^2} + \frac{w_b + w_s}{R_2} \tag{3b}$$

$$\gamma_{xy} = \frac{\partial u_0}{\partial y} + \frac{\partial v_0}{\partial x} - 2z\frac{\partial^2 w_b}{\partial x \partial y} - 2\Psi(z)\frac{\partial^2 w_s}{\partial x \partial y} \tag{3c}$$

$$\gamma_{xz} = g(z)\frac{\partial w_s}{\partial x} \tag{3d}$$

$$\gamma_{yz} = g(z)\frac{\partial w_s}{\partial y} \tag{3e}$$

In this work, a novel hyperbolic shear deformation plate theory of Houari is used [47].
In which

$$\Psi(z)=\frac{\left(1+2\,e+e^2\right)h\,\tanh(z/h)+4\,e\,z}{\left(1+2\,e+e^2\right)} \tag{3f}$$

$$g(z)=(1-\Psi'(z)) \tag{3g}$$

In the short form

$$\begin{Bmatrix}\varepsilon_x\\ \varepsilon_y\\ \gamma_{xy}\end{Bmatrix}=\begin{Bmatrix}\varepsilon_x^0\\ \varepsilon_y^0\\ \gamma_{xy}^0\end{Bmatrix}+z\begin{Bmatrix}k_x^b\\ k_y^b\\ k_{xy}^b\end{Bmatrix}+\Psi(z)\begin{Bmatrix}k_x^s\\ k_y^s\\ k_{xy}^s\end{Bmatrix} \tag{4a}$$

$$\begin{Bmatrix}\gamma_{yz}\\ \gamma_{xz}\end{Bmatrix}=\begin{Bmatrix}\gamma_{yz}^0\\ \gamma_{xz}^0\end{Bmatrix} \tag{4b}$$

In which

$$\begin{Bmatrix}\varepsilon_x^0\\ \varepsilon_y^0\\ \gamma_{xy}^0\end{Bmatrix}=\begin{Bmatrix}\dfrac{\partial u_0}{\partial x}+\dfrac{w_b+w_s}{R_1}\\ \dfrac{\partial v_0}{\partial y}+\dfrac{w_b+w_s}{R_2}\\ \dfrac{\partial u_0}{\partial y}+\dfrac{\partial v_0}{\partial x}\end{Bmatrix}, \tag{5a}$$

$$\begin{Bmatrix}k_x^b\\ k_y^b\\ k_{xy}^b\end{Bmatrix}=\begin{Bmatrix}-\dfrac{\partial^2 w_b}{\partial x^2}\\ -\dfrac{\partial^2 w_b}{\partial y^2}\\ -2\dfrac{\partial^2 w_b}{\partial x\partial y}\end{Bmatrix} \tag{5b}$$

$$\begin{Bmatrix}k_x^s\\ k_y^s\\ k_{xy}^s\end{Bmatrix}=\begin{Bmatrix}-\dfrac{\partial^2 w_s}{\partial x^2}\\ -\dfrac{\partial^2 w_s}{\partial y^2}\\ -2\dfrac{\partial^2 w_s}{\partial x\partial y}\end{Bmatrix} \tag{5c}$$

$$\begin{Bmatrix}\gamma_{yz}^0\\ \gamma_{xz}^0\end{Bmatrix}=g(z)\begin{Bmatrix}\dfrac{\partial w_s}{\partial x}\\ \dfrac{\partial w_s}{\partial y}\end{Bmatrix} \tag{5d}$$

For elastic and isotropic FGMs, the constitutive relations are given as follows

$$\begin{Bmatrix}\sigma_x\\ \sigma_y\\ \tau_{xy}\end{Bmatrix}=\begin{bmatrix}C_{11} & C_{12} & 0\\ C_{12} & C_{22} & 0\\ 0 & 0 & C_{66}\end{bmatrix}\begin{Bmatrix}\varepsilon_x\\ \varepsilon_y\\ \gamma_{xy}\end{Bmatrix} \tag{6a}$$

$$\begin{Bmatrix}\tau_{yz}\\ \tau_{xz}\end{Bmatrix}=\begin{bmatrix}C_{44} & 0\\ 0 & C_{55}\end{bmatrix}\begin{Bmatrix}\gamma_{yz}\\ \gamma_{xz}\end{Bmatrix} \tag{6b}$$

where

$$C_{11}=C_{22}=\frac{E(z)}{1-\nu^2},\quad C_{12}=\frac{\nu\,E(z)}{1-\nu^2},\quad C_{44}=C_{55}=C_{66}=\frac{E(z)}{2(1+\nu)} \tag{7}$$

In the present formulation, the parameter e denotes the Euler's number (e=exp(1)≈ 2.71828). The function $\psi(z)$ is constructed such that the transverse shear stresses vanish on the top and bottom surfaces of the shell, i.e., $g(\pm h/2)$, which eliminates the need for a shear correction factor in the proposed model. However, for the particular case where $\psi(z)=0$, the proposed theory reduces to the refined First-Order Shear Deformation Theory (RFSDT), and the shear correction factor is k_s =5/6 adopted to ensure consistency with classical results.

2.3 Governing equations

Considering the displacement components of the present simple new shear deformation theory in Eq. (2) and using the Principle of Minimum Total Potential Energy, the equations of motion of FG transparent shells resting on elastic foundation can be obtained as

$$\boldsymbol{\delta u}_0:\frac{\partial N_x}{\partial x}+\frac{\partial N_{xy}}{\partial y}=0 \tag{8a}$$

$$\boldsymbol{\delta v}_0:\frac{\partial N_{xy}}{\partial x}+\frac{\partial N_y}{\partial y}=0 \tag{8b}$$

$$\boldsymbol{\delta w_b}:\frac{\partial^2 M_x^b}{\partial x^2}+2\frac{\partial^2 M_{xy}^b}{\partial x\partial y}+\frac{\partial^2 M_y^b}{\partial y^2}-\frac{N_x}{R_1}-\frac{N_y}{R_2}+\overline{N}=0 \tag{8c}$$

$$\boldsymbol{\delta w_s}:\frac{\partial^2 M_x^s}{\partial x^2}+2\frac{\partial^2 M_{xy}^s}{\partial x\partial y}+\frac{\partial^2 M_y^s}{\partial y^2}+\frac{\partial Q_{xz}}{\partial x}+\frac{\partial Q_{yz}}{\partial y}-\frac{N_x}{R_1}-\frac{N_y}{R_2}+\overline{N}=0 \tag{8d}$$

$$\overline{N}=\left[N_x^0\frac{\partial^2 w_0}{\partial x^2}+N_y^0\frac{\partial^2 w_0}{\partial y^2}+2N_{xy}^0\frac{\partial^2 w_0}{\partial x\partial y}\right] \tag{9}$$

Where N_x^0, N_y^0 and $N_{x,y}^0$ are the membrane forces caused by in-plane end loads.
N_i, M_i, and Q_i are the local stress resultants which are calculated

$$\left(N_i,M_i\right)=\int_{-h/2}^{h/2}(1,z)\sigma_i dz \tag{10a}$$

$$\left(Q_x, Q_y\right) = k_s \int_{-h/2}^{h/2} g(z)\left(\tau_{xz}, \tau_{yz}\right) dz \tag{10b}$$

Upon substitution of Eq. (4) into Eq. (6) and the subsequent results into Eq. (10) the stress resultants are obtained in the matrix form as

$$\begin{Bmatrix} N_x \\ N_y \\ N_{xy} \end{Bmatrix} = \int_{-h/2}^{h/2} \begin{Bmatrix} \sigma_x \\ \sigma_y \\ \tau_{xy} \end{Bmatrix} dz = \mathbf{A}\ \boldsymbol{\varepsilon}^{\mathbf{0}} + \mathbf{B}\ \boldsymbol{\kappa}^{\mathbf{b}} + \mathbf{B}^{\mathbf{s}}\ \boldsymbol{\kappa}^{\mathbf{s}} \tag{11a}$$

$$\begin{Bmatrix} M_x^b \\ M_y^b \\ M_{xy}^b \end{Bmatrix} = \int_{-h/2}^{h/2} \begin{Bmatrix} \sigma_x \\ \sigma_y \\ \tau_{xy} \end{Bmatrix} z\, dz = \mathbf{B}\ \boldsymbol{\varepsilon}^{\mathbf{0}} + \mathbf{D}\ \boldsymbol{\kappa}^{\mathbf{b}} + \mathbf{D}^{\mathbf{s}}\ \boldsymbol{\kappa}^{\mathbf{s}} \tag{11b}$$

$$\begin{Bmatrix} M_x^s \\ M_y^s \\ M_{xy}^s \end{Bmatrix} = \int_{-h/2}^{h/2} \begin{Bmatrix} \sigma_x \\ \sigma_y \\ \tau_{xy} \end{Bmatrix} \Psi(z) dz = \mathbf{B}^{\mathbf{s}}\ \boldsymbol{\varepsilon}^{\mathbf{0}} + \mathbf{D}^{\mathbf{s}}\ \boldsymbol{\kappa}^{\mathbf{b}} + \mathbf{H}^{\mathbf{s}}\ \boldsymbol{\kappa}^{\mathbf{s}} \tag{11c}$$

$$\begin{Bmatrix} Q_{xz} \\ Q_{yz} \end{Bmatrix} = k_s \int_{-h/2}^{h/2} \begin{Bmatrix} \tau_{yz} \\ \tau_{xz} \end{Bmatrix} g(z)\, dz = \begin{bmatrix} A_{55}^s & 0 \\ 0 & A_{44}^s \end{bmatrix} \begin{Bmatrix} \gamma_{xz}^0 \\ \gamma_{yz}^0 \end{Bmatrix} = \mathbf{A}^{\mathbf{s}} \begin{Bmatrix} \partial w_s / \partial x \\ \partial w_s / \partial y \end{Bmatrix} \tag{11d}$$

where

$$\left(A_{ij}, B_{ij}, D_{ij}\right) = \int_{-h/2}^{h/2} C_{ij}\left(1, z, z^2\right) dz$$
$$\left(B_{ij}^s, D_{ij}^s, H_{ij}^s\right) = \int_{-h/2}^{h/2} C_{ij}\left(\Psi(z), \Psi(z) z, \Psi(z)^2\right) dz \tag{12a}$$

$$A_{ij}^s = k_s \int_{-h/2}^{h/2} C_{ij} g(z)^2\, dz, \quad i, j = 4,5 \tag{12b}$$

It is important to note that the shear correction factor k_s is not a universal constant but depends on the adopted kinematic model. For the proposed refined theory (with ψ(z) as defined in Eq. (3(f))), the shear correction factor is taken as k_s=1, as the transverse shear strain distribution $g(z)$ naturally satisfies the zero shear stress boundary conditions on the top and bottom surfaces. In the special case where ψ(z) =0, the theory reduces to the standard FSDT, and the classical value k_s=5/6 is employed. This distinction ensures a fair comparison between the proposed model and the RFSDT.

3. Analytical solution

Several analytical techniques are available for solving the governing equations of functionally graded shells. In the present study, Navier's method is employed to obtain closed-form solutions

for simply supported, doubly curved functionally graded transparent shells. The displacement fields are assumed in the following form

$$\begin{Bmatrix} u_0 \\ v_0 \\ w_b \\ w_s \end{Bmatrix} = \begin{Bmatrix} U_{mn}\cos(\alpha x)\sin(\beta y) \\ V_{mn}\sin(\alpha x)\cos(\beta y) \\ W_{bmn}\sin(\alpha x)\sin(\beta y) \\ W_{smn}\sin(\alpha x)\sin(\beta y) \end{Bmatrix} \tag{13}$$

where $\alpha = m\pi/\alpha$, $\beta = n\pi/b$ and (U_{mn}, V_{mn}, W_{bmn}, W_{smn}) are the unknown maximum displacement coefficients of the FG doubly curved shells.

Substituting Eq. (13) into Eq. (4) and then Eq. (8), one gets

$$[K]\{\Delta\} = 0 \tag{14}$$

where $\{\Delta\} = \{U_{mn}, V_{mn}, W_{bmn}, W_{smn}\}^t$ and $[K]$ is the symmetric matrix given by

$$[K] = \begin{bmatrix} a_{11} & a_{12} & a_{13} & a_{14} \\ a_{12} & a_{22} & a_{23} & a_{24} \\ a_{13} & a_{23} & a_{33} & a_{34} \\ a_{14} & a_{24} & a_{34} & a_{44} \end{bmatrix} \tag{15}$$

in which

$$\begin{aligned}
&a_{11} = -\left(A_{11}\alpha^2 + A_{66}\beta^2\right),\ a_{12} = -\alpha\beta\ (A_{12} + A_{66}),\\
&a_{13} = B_{11}\alpha^3 + \alpha\left((B_{12} + 2B_{66})\beta^2 + \frac{A_{11}}{R_1} + \frac{A_{12}}{R_2}\right),\ a_{14} = B^s_{11}\alpha^3 + \alpha\left(\left(B^s_{12} + 2B^s_{66}\right)\beta^2 + \frac{A_{11}}{R_1} + \frac{A_{12}}{R_2}\right),\\
&a_{22} = -\left(A_{22}\beta^2 + A_{66}\alpha^2\right),\ a_{23} = B_{22}\beta^3 + \alpha^2\beta(B_{12} + 2B_{66}) + \beta\left(\frac{A_{12}}{R_1} + \frac{A_{22}}{R_2}\right),\\
&a_{24} = B^s_{22}\beta^3 + \alpha^2\beta\left(B^s_{12} + 2B^s_{66}\right) + \beta\left(\frac{A_{12}}{R_1} + \frac{A_{22}}{R_2}\right),\\
&a_{33} = -\left(D_{11}\alpha^4 + D_{22}\beta^4 + 2\ (D_{12} + 2D_{66})\alpha^2\beta^2\right) - \left(\frac{B_{11}\alpha^2}{R_1} + \frac{B_{22}\beta^2}{R_2}\right)\\
&-2\frac{B_{12}\left(\alpha^2R_1^2R_2 + \beta^2R_1R_2^2\right)}{R_1^2R_2^2} - \left(\frac{A_{11}}{R_1^2} + 2\frac{A_{12}}{R_1R_2} + \frac{A_{22}}{R_2^2}\right) - 2N_x^0\alpha^2 - 2N_y^0\beta^2,\\
&a_{34} = -\left(D^s_{11}\alpha^4 + D^s_{22}\beta^4 + 2\ (D^s_{12} + 2D^s_{66})\alpha^2\beta^2\right) - \left(\frac{B_{11}\alpha^2}{R_1} + \frac{B_{22}\beta^2}{R_2}\right)\\
&-2\frac{B_{12}\left(\alpha^2R_1^2R_2 + \beta^2R_1R_2^2\right)}{R_1^2R_2^2} - \left(\frac{A_{11}}{R_1^2} + 2\frac{A_{12}}{R_1R_2} + \frac{A_{22}}{R_2^2}\right) - \left(\frac{B^s_{11}\alpha^2}{R_1} + \frac{B^s_{22}\beta^2}{R_2}\right)\\
&-2\frac{B^s_{12}\left(\alpha^2R_1^2R_2 + \beta^2R_1R_2^2\right)}{R_1^2R_2^2} - 2N_x^0\alpha^2 - 2N_y^0\beta^2,\\
&a_{44} = -\left(A^s_{55}\alpha^2 + A^s_{44}\beta^2 + \frac{A_{11}}{R_1^2} + 2\frac{A_{12}}{R_1R_2} + \frac{A_{22}}{R_2^2}\right) - \left(\frac{B^s_{11}\alpha^2}{R_1} + \frac{B^s_{22}\beta^2}{R_2}\right)\\
&-2\frac{B^s_{12}\left(\alpha^2R_1^2R_2 + \beta^2R_1R_2^2\right)}{R_1^2R_2^2} - \left(H^s_{11}\alpha^4 + H^s_{22}\beta^4 + 2\ (H^s_{12} + 2H^s_{66})\alpha^2\beta^2\right) - 2N_x^0\alpha^2 - 2N_y^0\beta^2.
\end{aligned} \tag{16}$$

Table 1. Comparison of nondimensional buckling load $\overline{N}_{cr} = N^0_{cr}\, a^2/\pi^2\, D$ of simply supported isotropic cylindrical panels (m = n = 1, ν = 0.3), $D = E\,h^3/12\left(1-\nu^2\right)$, $a/b = 1$, $E = 1\,GPa$

(γ_1, γ_2)	a/h	R_x/a	Matsunaga [48]	Ibka et al. [49]	Present
$(-1,0)$	10	∞	3.7412	3.7865	3.7422
		5	3.8391	3.8860	3.8357
		2,5	4.1283	4.1872	4.1211
	20	∞	3.9307	3.9444	3.9356
		5	4.3636	4.3804	4.3687
		2,5	5.6468	5.6981	5.6466
$(-1,-1)$	10	∞	1.8706	1.8932	1.8723
		5	1.9195	1.9430	1.9156
		2,5	2.0642	2.0936	2.0634
	20	∞	1.9654	1.9722	1.9676
		5	2.1818	2.1902	2.1833
		2,5	2.8234	2.8491	2.8256

By solving Eq. (16), closed-form analytical expressions for the critical buckling loads of the functionally graded, doubly curved shells are obtained.

4. Numerical results

4.1 Verification study

To validate the accuracy of the proposed formulation, the non-dimensional critical buckling load of a simply supported isotropic homogeneous spherical shell is first investigated. The shell is assumed to be simply supported along all four edges, and the obtained results are compared with those available in the literature to assess the accuracy and reliability of the present model.

Table 1 presents the non-dimensional critical buckling loads under in-plane loading predicted by the proposed hyperbolic shear deformation theory (HypSDT). The results are compared with those reported by Matsunaga [48] using HSDT and with the refined FSDT developed by Ibka et al. [49]. Excellent agreement is observed, confirming the accuracy and reliability of the proposed formulation for the buckling analysis of doubly curved shells.

Table 2 compares the non-dimensional critical buckling loads $\overline{N}_{cr}$ of various shallow curved shells subjected to uniaxial and biaxial uniformly distributed edge loads with the benchmark results reported by Al Mukahal et al. [50] and Basoglu et al. [34] for different R_x/a and R_y/b ratios. The excellent agreement between the present predictions and the published results demonstrates the accuracy and reliability of the proposed theoretical formulation for the buckling analysis of shallow curved shells.

As presented in Table 3, the predicted buckling loads agree remarkably well with the benchmark solutions obtained using HSDT [48], FSDT [51], [52], and the refined FSDT

Table 2. Comparison of nondimensional buckling load $\overline{N}_{cr} = N^0_{cr}\, a^2/\pi^2\, D$ of various curved shallow shells (m = n = 1, ν = 0.3), $D = E\,h^3/12\left(1-\nu^2\right)$, $a/b = 1$, $E = 1\,GPa$

(γ_1, γ_2)	R_x/a	R_y/b	Al Mukahal et al. [50]	Basoglu et al. [34]	Present
$(-1,0)$	∞	∞	3.7866	3.7884	3.7898
	5	5	4.2350	4.2371	4.2256
	5	∞	3.8987	3.9005	3.8971
	5	−5	3.7866	3.7884	3.7813
$(-1,-1)$	∞	∞	1.8933	1.8942	1.8944
	5	5	2.1175	2.1185	2.1165
	5	∞	1.9493	1.9503	1.9489
	5	−5	1.8933	1.8942	1.8965

Table 3. Comparison of buckling loads $\hat{N}_{cr} = N^0_{cr}\, a^2/D$ for isotropic shallow curved panels ($a/b = 1$ and ν = 0.3)

Types	a/h	Matsunaga [48]	Sahu and Datta [52]	Ravi Kumar et al. [51]	Nandun et al. [53]	Present
SP shells	10	41.0872	41.0487	41.0487	41.5987	41.0467
	20	56.1620	56.2143	56.2143	56.4272	56.1652
HP shells	10	36.6162	36.5235	36.5235	37.0651	36.6145
	20	38.5033	38.4618	38.4618	38.6137	38.5028
CY shells	10	37.8904	37.8075	37.8075	38.3513	37.8975
	20	43.0670	43.0581	43.0581	43.2249	43.0691
FL Plates	10	36.9242	36.8284	36.8284	37.3708	36.9274
	20	38.7945	38.7757	38.7757	38.9295	38.7965

developed by Nandun et al. [53], confirming the accuracy and reliability of the proposed formulation.

4.2 Parametric study

For the parametric study, a functionally graded (FG) transparent doubly curved shell composed of sapphire and sodalime glass is considered. This material combination is well suited for transparent structural applications because sapphire exhibits exceptionally high stiffness and strength ($E_c = 345\,GPa$), whereas soda–lime glass has a lower Young's modulus ($E_m = 70\,GPa$) but offers excellent optical transparency and is widely used in architectural glazing systems ($\nu_m = \nu_c = 0.23$) as in Touloukian et al. [54].

The continuous through thickness gradation of material properties allows the functionally graded shell to achieve an effective balance between the superior mechanical characteristics of sapphire and the excellent optical transparency of sodalime glass. Unlike conventional laminated configurations, the absence of discrete material interfaces ensures a smooth transition in material properties, thereby minimizing stress concentrations, enhancing load transfer efficiency, and improving the overall structural integrity and long-term durability of the shell.

Table 4: Comparison of the nondimensional buckling load $\widehat{N}_{cr} = N_{cr}^{0}\, a^2/\pi^2\, D_c$ of the FG doubly curved shells, $D_c = E\,h^3/12\left(1-\nu^2\right)$, $a/h = 10$

(γ_1,γ_2)	Types	k					
		0	0.5	1	2	5	10
$(-1,0)$	FL Plates	3.80854	2.52986	1.96740	1.56509	1.32976	1.20543
	SP shells	4.25984	2.82657	2.23014	1.76754	1.47365	1.32267
	HP shells	3.78735	2.49021	1.95270	1.55256	1.31907	1.19566
	CY shells	3.94532	2.59004	2.02745	1.61070	1.36132	1.23123
$(-1,-1)$	FL Plates	1.91254	1.25698	0.98423	0.78259	0.66487	0.60276
	SP shells	2.11567	1.41976	1.11545	0.88378	0.73630	0.66154
	HP shells	1.88546	1.24766	0.97555	0.77631	0.65959	0.59787
	CY shells	1.95923	1.29443	1.01387	0.80545	0.68063	0.61560

The nondimensional critical buckling loads $\widehat{N}_{cr}$ of FG transparent doubly curved shells are presented in Table 3 for different values of the power-law index k under both uniaxial and biaxial uniformly distributed edge loads. The results are reported for several shell geometries, including flat plates (FL), spherical shells (SP), hyperbolic paraboloid shells (HP), and cylindrical shells (CY). In which, the dimensions of the shells are $a/h = 10$, $R_x = R_y = \infty$ for FL plates, $R_x/a = R_y/b = 5$ for SP shells, $R_x/a = -R_y/b = 5$ for HP shells, $R_x/a = 5$, $R_y = \infty$ for CY shells.

As shown in Table 4, the non-dimensional critical buckling load, $\widehat{N}_{cr}$, decreases progressively as the power-law index k increases. This behavior is directly related to the variation of material properties through the shell thickness. For $k = 0$, the shell is composed entirely of sapphire, whose high Young's modulus provides superior stiffness and, consequently, greater resistance to buckling. As k increases, the volume fraction of soda–lime glass gradually increases while that of sapphire decreases, leading to a reduction in the overall stiffness of the shell. As a result, the critical buckling load decreases because the structure becomes more flexible.

Table 4 also highlights the significant influence of shell geometry on buckling performance. Among the configurations investigated, spherical (SP) shells exhibit the highest non-dimensional critical buckling loads owing to their balanced double curvature, which enhances membrane action and significantly increases structural stiffness and stability. In contrast, flat (FL) plates and hyperbolic paraboloid (HP) shells exhibit lower buckling loads because of their relatively lower geometric stiffness. Cylindrical (CY) shells display intermediate behavior, with buckling capacities lying between those of spherical shells and flat plates. It is also evident that the non-dimensional critical buckling loads under biaxial compression are consistently lower than those under uniaxial compression. This behavior is expected, as simultaneous compression along two orthogonal directions increases the susceptibility of the shell to instability, resulting in earlier buckling. Overall, the results confirm that both the material gradation index and the shell geometry are key parameters governing the stability performance of functionally graded transparent shell structures.

Figs. 3-6 illustrate the influence of key geometric parameters on the nondimensional critical buckling load $\widehat{N}_{cr} = N_{cr}^{0}\, a^2/\pi^2\, D_c$ with $D_c = E\,h^3/12\left(1-\nu^2\right)$ of functionally graded doubly curved transparent shells under uniaxial and biaxial compression.

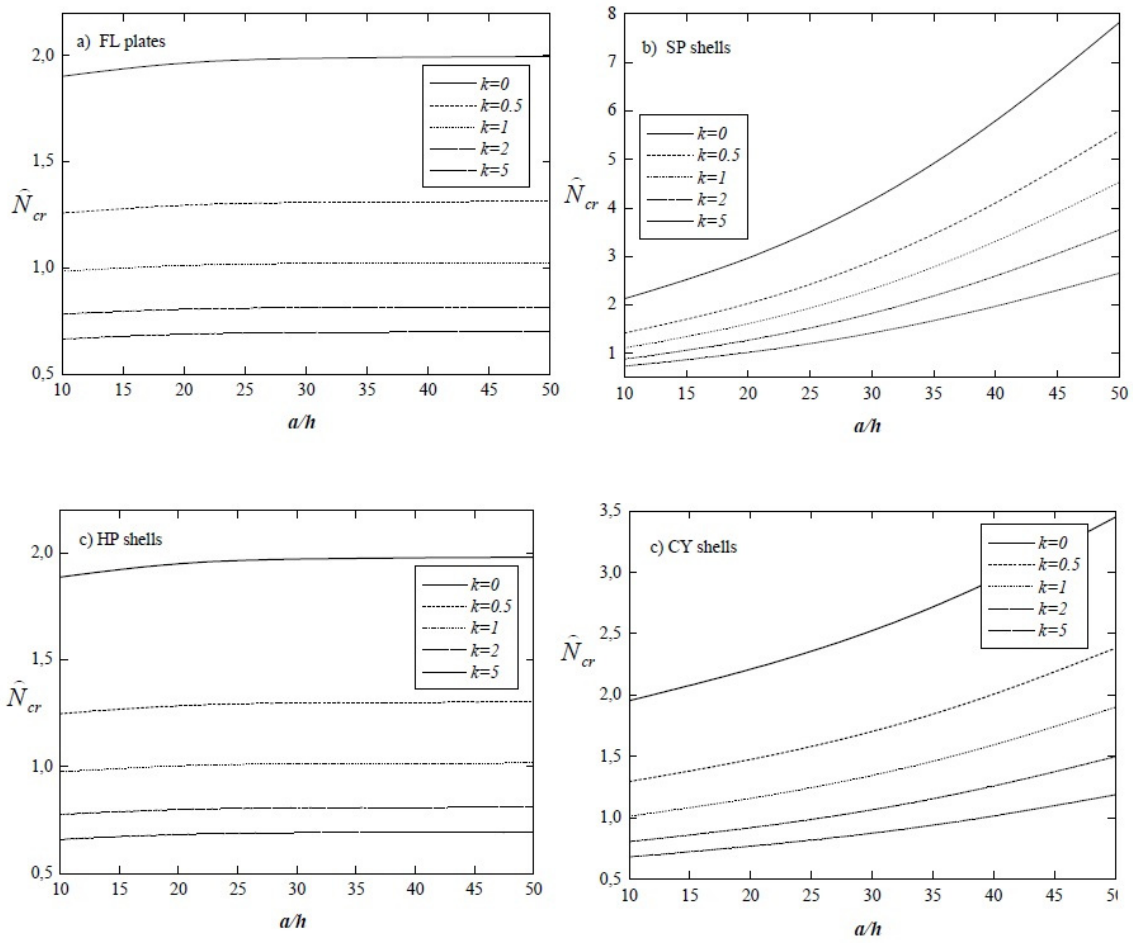

Figure 3. The variation of the nondimensional critical buckling load $\hat{N}_{cr}$ of FG doubly curved shells versus the side-to-thickness ratio

As shown in Fig. 3, $\hat{N}_{cr}$ increases significantly with the side-to-thickness ratio a/h, reflecting the transition from shear-dominated thick-shell behavior to membrane-dominated thin-shell response; spherical shells (SP) consistently exhibit the highest values, while higher power-law indices k lead to a marked reduction in buckling resistance due to increased compliance from the soda-lime glass phase.

Fig. 4 reveals that $\hat{N}_{cr}$ decreases with rising radius-to-side ratio R/a, as larger radii diminish the stabilizing effect of curvature and approach flat-plate behavior; SP and cylindrical (CY) configurations remain superior for $R/a < 5$.

In Fig. 5, the buckling load is minimized near aspect ratio $a/b \approx 1$ (square geometry) and rises for elongated panels, with the advantage of SP shells diminishing as a/b increases; strong gradients ($k > 2$) amplify sensitivity to this parameter.

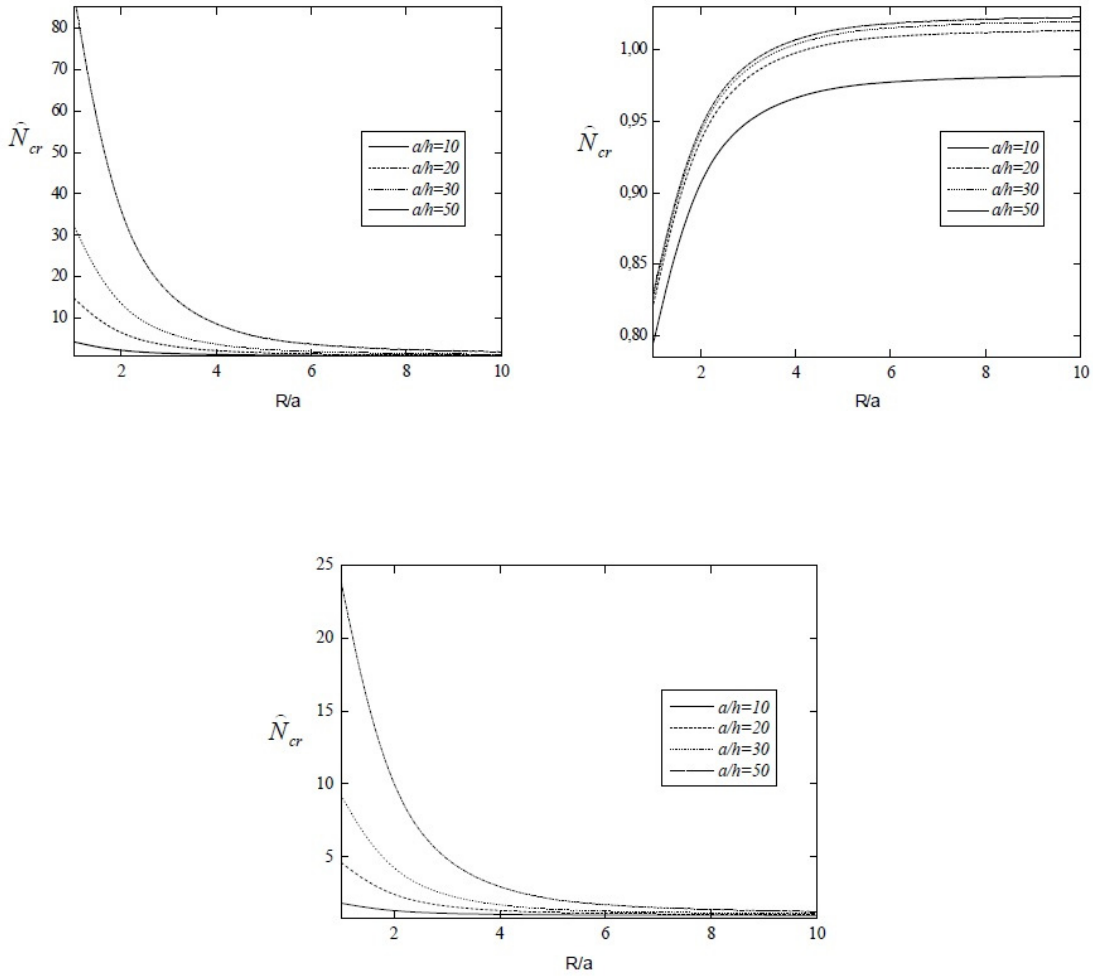

Figure 4. The variation of the nondimensional critical buckling load $\hat{N}_{cr}$ of FG doubly curved shells versus the radius-to-side ratio

Finally, Fig. 6 demonstrates that maximum stability occurs at radius ratio R_1/R_2 (symmetric spherical shells), with any deviation reducing $\hat{N}_{cr}$, particularly for hyperbolic paraboloid (HP) shells and higher k values. Overall, these results highlight the critical role of balanced double curvature, moderate thickness ratios, and low material gradation ($k < 2$) in enhancing buckling performance, providing valuable guidance for the design of lightweight, transparent FG panels in architectural curtain walls and aerospace applications. The pronounced increase in the critical buckling load for spherical shells is attributed to the membrane-stiffening effect generated by balanced double curvature. As the shell tends toward a cylindrical geometry, the curvature in one principal direction disappears, reducing the geometric stiffness and consequently lowering the buckling resistance.

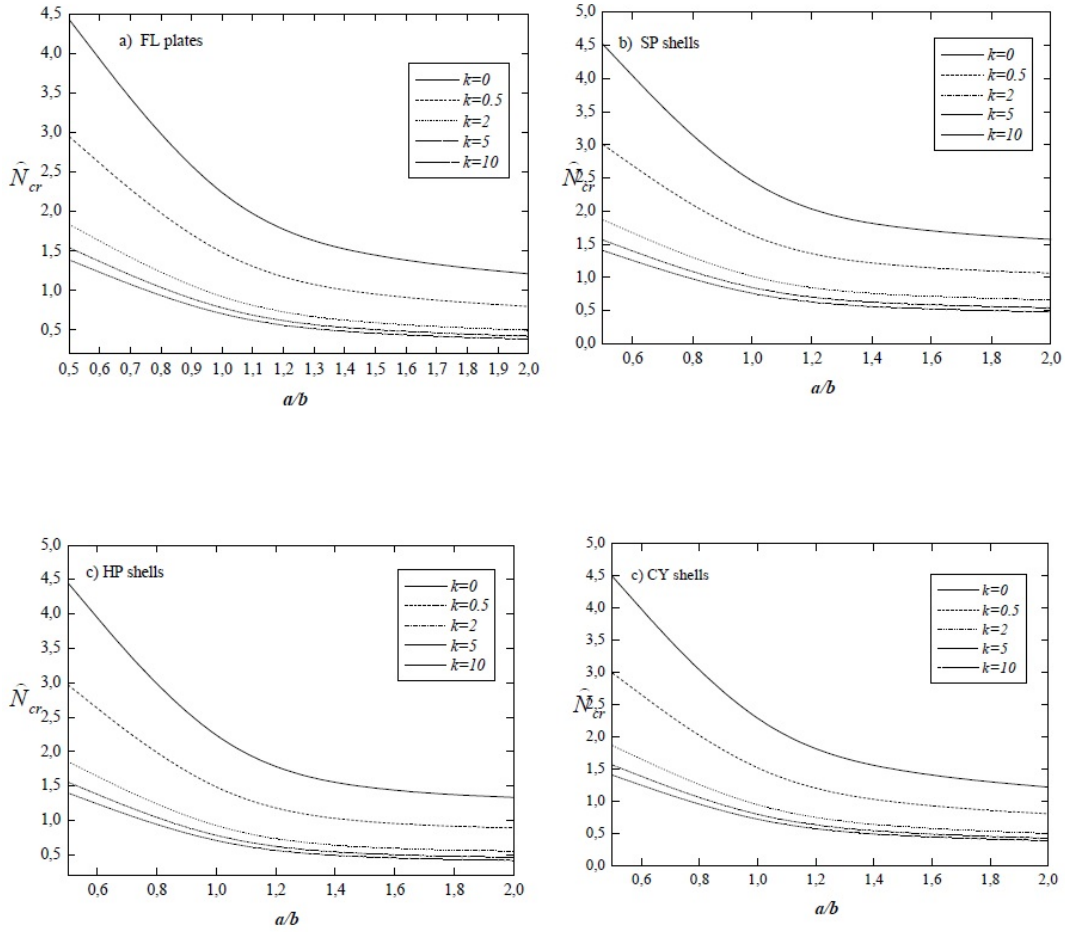

Figure 5. The variation of the nondimensional critical buckling load $\widehat{N}_{cr}$ of FG doubly curved shells versus the aspect ratio

4. Conclusions

This study presented a refined four-variable Hyperbolic Shear Deformation Theory (HypSDT) for the mechanical buckling analysis of functionally graded (FG) transparent doubly curved shells. Based on the numerical investigations, the following conclusions can be drawn:

- The proposed four-variable formulation provides an accurate and computationally efficient alternative to the conventional theories for predicting the buckling response of thin-to-moderately thick FG transparent shells.
- Validation against well-established analytical and numerical solutions reported in the literature demonstrated excellent agreement, confirming the accuracy and reliability of the proposed model.
- Shell geometry plays a key role in structural stability. Among the configurations examined, spherical shells exhibit the highest buckling resistance owing to their balanced double

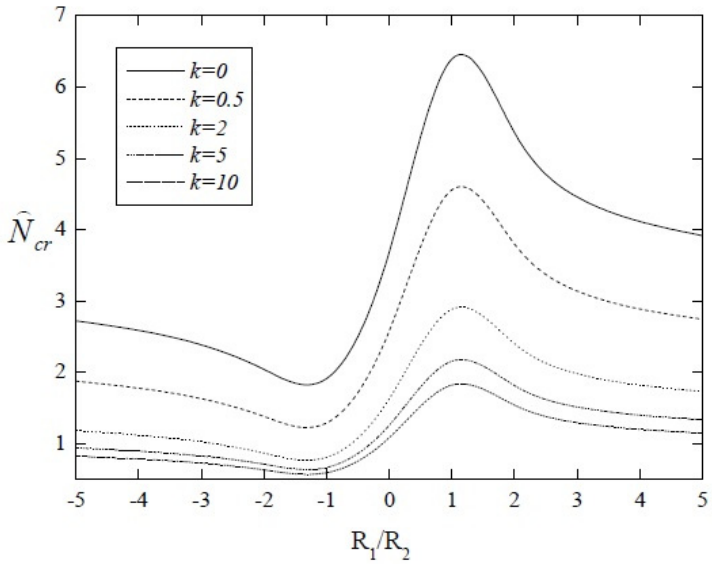

Figure 6. The variation of the nondimensional critical buckling load $\widehat{N}_{cr}$ of FG doubly curved shells versus the aspect ratio

curvature, whereas cylindrical, hyperbolic paraboloid, and flat shells show progressively lower critical buckling loads.

- The critical buckling load increases with the side-to-thickness ratio a/h and decreases as the aspect ratio a/b increases, highlighting the important influence of geometric parameters on the stability performance of FG transparent shells.
- The proposed formulation offers an efficient framework for the buckling analysis of FG transparent shell structures subjected to simply supported boundary conditions. However, the present work is limited to linear elastic buckling and does not consider geometric nonlinearities, post-buckling behavior, thermo-mechanical effects, dynamic loading, material degradation, or arbitrary boundary conditions.

Future work will focus on extending the proposed formulation to nonlinear and post-buckling analyses, thermo-mechanical and dynamic loading conditions, and experimental validation. In addition, the analytical framework will be generalized to accommodate more realistic boundary conditions by adopting solution procedures similar to those proposed by Liu et al. [54], [55], thereby broadening the applicability of the present model to practical transparent shell structures.

References

1. Cuce, E., Young, C.H., Riffat, S.B. (2015). Thermal performance investigation of heat insulation solar glass: A comparative experimental study. Energy and Buildings, 86, 595-600. https://doi.org/10.1016/j.enbuild.2014.10.063.
2. Ünlütürk, M.S., Kazanasmaz, T. (2024). Integration of daylight use and analysis in double skin facades:

a literature review. Gazi University Journal of Science, 37(2), 520-544. https://doi.org/10.35378/gujs.1243933.

3. She, G.L., Xu, J.Q. (2025). Nonlinear resonance and chaos in rotating functionally graded carbon nanotube-reinforced composite annular plates. Advances in Aircraft and Spacecraft Science, 12(1), 77-93. https://doi.org/10.12989/aas.2025.12.1.077.
4. Houari, M.S.A., Belhocine, A., Daikh, A.A., Belarbi, M.O., Merzouki, T., Tounsi, A. (2025). A refined integral parabolic plate theory incorporating stretching effects for free vibration analysis of advanced composite plates on Winkler-Pasternak foundation. Earthquakes and Structures, 29(3), 165-174. https://doi.org/10.12989/eas.2025.29.3.165.
5. Wei, Y.Y., Al-Furjan, M.S.H., Shan, L., Shen, X., Kolahchi, R., Rabani Bidgoli, M., Farrokhian, A. (2024). Micro-mass sensor-based vibration response of smart bidirectional functionally graded auxetic microbeams. Archives of Civil and Mechanical Engineering, 24(1), 38. https://doi.org/10.1007/s43452-023-00840-2.
6. Meksi, A., Draiche, K., Madenci, E., Tounsi, A. (2025). A new higher-order displacement model for laminated composite cylindrical shells. Advances in Aircraft and Spacecraft Science, 12(2), 117-139. https://doi.org/10.12989/aas.2025.12.2.117.
7. Shaikh, A.S., Sayyad, A.S. (2025). Refined 6-DOF hyperbolic model for the free vibration analysis of multi-layered sandwich shallow shells. Advances in Aircraft and Spacecraft Science, 12(4), 315. https://doi.org/10.12989/aas.2025.12.4.315.
8. Liu, Y., Vella, D., Qin, Z., Chu, F., Amabili, M. (2026). A review of nonlinear dynamics and vibration in lightweight composite structures: Recent advances and challenges. Engineering Structures, 360, 122835. https://doi.org/10.1016/j.engstruct.2026.122835.
9. Alashkar, A., Elkafrawy, M., Hawileh, R., AlHamaydeh, M. (2024). Elastic buckling behavior of functionally graded material thin skew plates with circular openings. Buildings, 14(3), 572. https://doi.org/10.3390/buildings14030572.
10. Arefi, M. (2015). The effect of different functionalities of FGM and FGPM layers on free vibration analysis of the FG circular plates integrated with piezoelectric layers. Smart Structures and Systems, 15(5), 1345-1362. https://doi.org/10.12989/sss.2015.15.5.1345.
11. Darilmaz, K. (2015). Vibration analysis of functionally graded material (FGM) grid systems. Steel and Composite Structures, 18(2), 395-408. https://doi.org/10.12989/scs.2015.18.2.395.
12. Pradhan, K.K., Chakraverty, S. (2015). Free vibration of functionally graded thin elliptic plates with various edge supports. Structural Engineering and Mechanics, 53(2), 337-354. https://doi.org/10.12989/sem.2015.53.2.337.
13. Moita, J.S., Araújo, A.L., Correia, V.F., Soares, C.M.M. (2021). Mechanical and thermal buckling of functionally graded axisymmetric shells. Composite Structures, 261, 113318. https://doi.org/10.1016/j.compstruct.2020.113318.
14. Turan, F. (2022). Stability of the porous orthotropic laminated composite plates via the hyperbolic shear deformation theory. Steel and Composite Structures, 48(2), 145-161. https://doi.org/10.12989/scs.2023.48.2.145.
15. Turan, F. (2024). Free vibration response of multi-layered plates with trigonometrically distributed porosity based on the higher-order shear deformation theory. Steel and Composite Structures, 53(1), 77-90. https://doi.org/10.12989/scs.2024.53.1.077.
16. Turan, F., Ertek, M.K., Köktan, U., Basoglu, M.F. (2026). Buckling response of porous orthotropic laminated plates subjected to non-uniform edge compressions: Effect of orthotropic foundations. Thin-Walled Structures, 218, 114122. https://doi.org/10.1016/j.tws.2025.114122.
17. Turan, F., Bahadır, F.C., Chaabani, H. (2025). Analysis of higher-order shear deformable porous orthotropic laminated doubly-curved shallow shells with non-uniformly distributed porosity: Nonlinear free vibration response. Engineering Structures, 343, 121074. https://doi.org/10.1016/j.engstruct.2025.121074.
18. Turan, F., Ertek, M.K., Köktan, U., Karadeniz, M., Zeren, E., Basoglu, M.F. (2026). Effect of orthotropic Pasternak foundation on free vibration of porous orthotropic laminated plates. International

Journal of Mechanics and Materials in Design, 22(1). https://doi.org/10.1007/s10999-025-09863-4.
19. Wang, Q., Shao, D., Qin, B. (2018). A simple first-order shear deformation shell theory for vibration analysis of composite laminated open cylindrical shells with general boundary conditions. Composite Structures, 184, 211-232. https://doi.org/10.1016/j.compstruct.2017.09.070.
20. Van Vinh, P., Tounsi, A. (2022). Free vibration analysis of functionally graded doubly curved nanoshells using nonlocal first-order shear deformation theory with variable nonlocal parameters. Thin-Walled Structures, 174, 109084. https://doi.org/10.1016/j.tws.2022.109084.
21. Madani, H., Hosseini, H., Shokravi, M. (2016). Differential cubature method for vibration analysis of embedded FG-CNT-reinforced piezoelectric cylindrical shells subjected to uniform and non-uniform temperature distributions. Steel and Composite Structures, 22(4), 889-913. http://dx.doi.org/10.12989/scs.2016.22.4.889
22. Qin, Z., Zhao, S., Pang, X., Safaei, B., Chu, F. (2020). A unified solution for vibration analysis of laminated functionally graded shallow shells reinforced by graphene with general boundary conditions. International Journal of Mechanical Sciences, 170, 105341. https://doi.org/10.1016/j.ijmecsci.2019.105341.
23. Li, H., Pang, F., Chen, H., Du, Y. (2019a). Vibration analysis of functionally graded porous cylindrical shell with arbitrary boundary restraints by using a semi analytical method. Composites Part B: Engineering, 164, 249-264. https://doi.org/10.1016/j.compositesb.2018.11.046.
24. Li, H., Pang, F., Miao, X., Gao, S., Liu, F. (2019b). A semi analytical method for free vibration analysis of composite laminated cylindrical and spherical shells with complex boundary conditions. Thin-Walled Structures, 136, 200-220. https://doi.org/10.1016/j.tws.2018.12.009.
25. Kar, V.R., Panda, S.K., Mahapatra, T.R. (2016). Thermal buckling behaviour of shear deformable functionally graded single/doubly curved shell panel with TD and TID properties. Advances in Materials Research, 5(4), 205. https://doi.org/10.12989/amr.2016.5.4.205.
26. Kar, V.R., Mahapatra, T.R., Panda, S.K. (2017). Effect of different temperature load on thermal postbuckling behaviour of functionally graded shallow curved shell panels. Composite Structures, 160, 1236-1247. https://doi.org/10.1016/j.compstruct.2016.10.125.
27. Kar, V.R., Panda, S.K. (2015). Nonlinear flexural vibration of shear deformable functionally graded spherical shell panel. Steel and Composite Structures, 18(3), 693-709. https://doi.org/10.12989/scs.2015.18.3.693.
28. Liu, Y., Qin, Z., Chu, F. (2021). Nonlinear forced vibrations of functionally graded piezoelectric cylindrical shells under electric-thermo-mechanical loads. International Journal of Mechanical Sciences, 201, 106474. https://doi.org/10.1016/j.ijmecsci.2021.106474.
29. Turan, F., Karadeniz, M., Zeren, E. (2024). Free vibration and buckling behavior of porous orthotropic doubly-curved shallow shells subjected to non-uniform edge compression using higher-order shear deformation theory. Thin-Walled Structures, 205, 112522. https://doi.org/10.1016/j.tws.2024.112522.
30. Turan, F., Karadeniz, M., Zeren, E., Hoang, V.N.V. (2025). Porous orthotropic shallow shells: Nonlinear vibration and post-buckling under non-uniform edge loads. Thin-Walled Structures, 113845. https://doi.org/10.1016/j.tws.2025.113845.
31. Turan, F., Zeren, E., Basoglu, M.F., Köktan, U., Ertek, M.K. (2026). Coupled effects of porosity and orthotropic foundations on the fundamental frequency characteristics of orthotropic laminated doubly curved shallow shells. Mechanics of Advanced Materials and Structures, 33(1), 2621933. https://doi.org/10.1080/15376494.2026.2621933.
32. Turan, F., Zeren, E., Karadeniz, M., Basoglu, M.F. (2025). Analysis of higher-order shear deformable porous orthotropic laminated doubly-curved shallow shells subjected to non-uniformly distributed edge loadings: Nonlinear post-buckling response. Thin-Walled Structures, 113878. https://doi.org/10.1016/j.tws.2025.113878.
33. Turan, F., Zeren, E., Karadeniz, M., Hoang, V.N.V. (2025). Natural frequencies of shear deformable porous orthotropic laminated doubly-curved shallow shells with non-uniformly distributed porosity using higher-order shear deformation theory. Thin-Walled Structures, 210, 112951.

https://doi.org/10.1016/j.tws.2025.112951.
34. Basoglu, M.F., Bahadır, F.C., Turan, F. (2025). Buckling response of porous orthotropic laminated doubly-curved shallow shells subjected to non-uniform edge compressions using trigonometric shear deformation theory. Engineering Structures, 336, 120359. https://doi.org/10.1016/j.engstruct.2025.120359.
35. Keleshteri, M. M., & Jelovica, J. J. E. S. (2022). Analytical solution for vibration and buckling of cylindrical sandwich panels with improved FG metal foam core. Engineering Structures, 266, 114580. https://doi.org/10.1016/j.engstruct.2022.114580
36. Benounas, S., Belarbi, M.O., Van, V.P., Daikh, A.A. (2024). Precise analysis of the static bending response of functionally graded doubly curved shallow shells via an improved finite element shear model. Engineering Structures, 319, 118829. https://doi.org/10.1016/j.engstruct.2024.118829.
37. Han, G., Wan, M., Su, A., Li, B. (2025). Thermal buckling and post-buckling behavior of FGM laminate plates reinforced with graphene nanoplatelets. Multiscale and Multidisciplinary Modeling, Experiments and Design, 8(5), 256. https://doi.org/10.1007/s41939-025-00810-6.
38. Carrera, E., Brischetto, S. (2008). Analysis of thickness locking in classical, refined and mixed theories for layered shells. Composite Structures, 85(1), 83-90. https://doi.org/10.1016/j.compstruct.2007.10.009.
39. Thai, H.T., Choi, D.H. (2013). Efficient higher-order shear deformation theories for bending and free vibration analyses of functionally graded plates. Archive of Applied Mechanics, 83, 1755-1771. https://doi.org/10.1007/s00419-013-0776-z.
40. Jung, W.Y., Han, S.C., Park, W.T. (2016). Four-variable refined plate theory for forced-vibration analysis of sigmoid functionally graded plates on elastic foundation. International Journal of Mechanical Sciences, 111, 73-87. https://doi.org/10.1016/j.ijmecsci.2016.03.001.
41. Fahsi, A., Tounsi, A., Hebali, H., Chikh, A., Bedia, E.A., Mahmoud, S.R. (2017). A four variable refined nth-order shear deformation theory for mechanical and thermal buckling analysis of functionally graded plates. Geomechanics and Engineering, 13(3), 385-410. https://doi.org/10.12989/gae.2017.13.3.385.
42. Arefi, M., Mohammad-Rezaei Bidgoli, E., Civalek, O. (2022). Bending response of FG composite doubly curved nanoshells with thickness stretching via higher-order sinusoidal shear theory. Mechanics Based Design of Structures and Machines, 50(7), 2350-2378. https://doi.org/10.1080/15397734.2020.1777157.
43. Civalek, O., Jalaei, M.H. (2020). Shear buckling analysis of functionally graded (FG) carbon nanotube reinforced skew plates with different boundary conditions. Aerospace Science and Technology, 99, 105753. https://doi.org/10.1016/j.ast.2020.105753.
44. Arshid, E., Nia, M.J.M., Ghorbani, M.A., Civalek, Ö., Kumar, A. (2023). On the poroelastic vibrations of lightweight FGSP doubly-curved shells integrated with GNPs-reinforced composite coatings in thermal atmospheres. Applied Mathematical Modelling, 124, 122-141. https://doi.org/10.1016/j.apm.2023.07.036.
45. Carrera, E., Zozulya, V.V. (2023). Carrera unified formulation (CUF) for the shells of revolution. II. Navier close form solutions. Acta Mechanica, 234(1), 137. https://doi.org/10.1007/s00707-022-03373-6.
46. Muthanna, A., Ali, M., Hasan, H. M., Najim, K.B., Njim, E.K., Madan, R., Al-Maamori, M.H. (2025). Vibration investigation of an imperfect FGM cylindrical shell reinforced by various types of stiffeners with temperature-dependent properties resting on an elastic foundation. Coupled Systems Mechanics, 14(2), 105-127. https://doi.org/10.12989/csm.2025.14.2.105.
47. Bakoura, A., Remil, A., Bessaim, A., Houari, M.S.A., Meriem, S., Soufiane, I.M., Tounsi, A. (2026). Mechanical and thermal buckling analysis of P-FG plate using an innovative HSDT and Airy stress function. Coupled Systems Mechanics, 15(2), 135-155. https://doi.org/10.12989/csm.2026.15.2.135
48. Matsunaga, H. (1999). Vibration and stability of thick simply supported shallow shells subjected to in-plane stresses. Journal of Sound and vibration, 225(1), 41-60. https://doi.org/10.1006/jsvi.1999.2234.
49. Ibka, M.S., Mokhefi, D., Bessaim, A., Megaiz, M., Guendouz, I., Bakoura, A., Belhocine, A., Houari, M.S.A. (2026). A novel four-variable FSDT approach for mechanical buckling analysis of functionally

graded transparent shell structures. Coupled Systems Mechanics, (in press).
50. Al Mukahal, F.H., Abazid, M.A., Sobhy, M. (2023). Investigating electromechanical buckling response of FG-GPL-reinforced piezoelectric doubly curved shallow shells embedded in an elastic substrate. Materials, 16(8), 2975. https://doi.org/10.3390/ma16082975.
51. Ravi Kumar, L., Datta, P.K., Prabhakara, D.L. (2002). Tension buckling and vibration behaviour of curved panels subjected to non-uniform in-plane edge loading. International Journal of Structural Stability and Dynamics, 2(3), 409-423. https://doi.org/10.1142/S0219455402000579.
52. Sahu, S.K., Datta, P.K. (2001). Parametric instability of doubly curved panels subjected to non-uniform harmonic loading. Journal of Sound and Vibration, 240(1), 117-129. https://doi.org/10.1006/jsvi.2000.3187.
53. Nandun, H., Jiammeepreecha, W., Roun, S., Wattanasakulpong, N., Phungpaingam, B., Mahasuwanchai, P., Jaturapitakkul, C. (2026). An appraisal of Voigt and Mori–Tanaka models for free vibration and buckling analyses of FG shallow curved shell panels reinforced with GPLs and resting on Kerr foundation using an improved FSDT. Mechanics Based Design of Structures and Machines, 54(1). https://doi.org/10.1080/15397734.2026.2696003.
54. Touloukian, Y.S., Kirby, R.K., Taylor, R.E., Desai, P.D. (1977). Thermophysical properties of matter – Vol. 13: Thermal Expansion; Vol. 2: Thermal Conductivity. IFI/Plenum, New York.
55. Liu, Y., Qin, Z., Chu, F. (2022b). Investigation of magneto-electro-thermo-mechanical loads on nonlinear forced vibrations of composite cylindrical shells. Communications in Nonlinear Science and Numerical Simulation, 107, 106146. https://doi.org/10.1016/j.cnsns.2021.106146.
56. Liu, Y., Zhu, R., Qin, Z., Chu, F. (2022a). A comprehensive study on vibration characteristics of corrugated cylindrical shells with arbitrary boundary conditions. Engineering Structures, 269, 114818. https://doi.org/10.1016/j.engstruct.2022.114818.